

Synchrotron and Smith-Purcell radiations from a charge rotating around a cylindrical grating

A. A. Saharian^{1,2}, A. S. Kotanjyan², A. R. Mkrtchyan^{1,3}, B. V. Khachatryan^{1,2}

¹*Institute of Applied Problems in Physics NAS RA,
25 Nersessian Street, 0014 Yerevan, Armenia*

²*Department of Physics, Yerevan State University,
1 Alex Manoogian Street, 0025 Yerevan, Armenia*

³*Tomsk Polytechnic University, 30 Lenin Avenue, 634050 Tomsk, Russia*

September 28, 2018

Abstract

We investigate the radiation from a charge rotating around conductors with cylindrical symmetry. First the problem is considered with a charge rotating around a conducting cylinder immersed in a homogeneous medium. The surface charge and current densities induced on the cylinder surface are evaluated. A formula is derived for the spectral-angular density of the radiation intensity. In the second part, we study the radiation for a charge rotating around a diffraction grating on a cylindrical surface with metallic strips parallel to the cylinder axis. The effect of the grating on the radiation intensity is approximated by the surface currents induced on the strips by the field of the rotating charge. The expressions are derived for the electric and magnetic fields and for the angular density of the radiation intensity on a given harmonic. We show that the interference between the synchrotron and Smith-Purcell radiations may lead to interesting features. In particular, the behavior of the radiation intensity on large harmonics can be essentially different from that for a charge rotating in the vacuum or around a solid cylinder. Unlike to these limiting cases, for the geometry of diffraction grating the radiation intensity on higher harmonics does not vanish for small angles with respect to the cylinder axis. For given characteristics of the charge, by the choice of the parameters of the diffraction grating, one can have highly directional radiation near the normal to the plane of the charge rotation. With decreasing energy, the relative contribution of the synchrotron radiation decreases and the Smith-Purcell part is dominant.

1 Introduction

Due to its unique characteristics, such as broad spectrum, high flux, and high degree of polarization, the synchrotron radiation (for reviews see [1]-[5]) is an ideal tool for many types of research and also has found industrial applications including materials science, biological and life sciences, medicine, chemistry. These extensive applications motivate the importance of investigations for various types of mechanisms to control the radiation parameters. In particular, it is of interest to consider the influence of a medium on the spectral-angular characteristics of the radiation intensity. The synchrotron radiation from a charged particle circulating in a homogeneous and isotropic medium was considered in [6, 7, 8], where it has been shown that the interference between the synchrotron and Cherenkov radiations leads to remarkable effects. In particular, for high-energy particles and close to the Cherenkov threshold the total radiation rate oscillates.

New interesting features arise for the synchrotron radiation in inhomogeneous media. As an exactly solvable problem of this kind, in [9], we have studied the radiation from a charge orbiting around/inside a dielectric cylinder immersed into a homogeneous medium. Under the Cherenkov condition for the material of the cylinder and for the velocity of the particle image on the cylinder surface, strong narrow peaks appear in the angular distribution of the radiation intensity at large distances from the cylinder. At these peaks the radiated energy exceeds the corresponding quantity in the case of a homogeneous medium by several orders of magnitude. It has been shown that the angular locations of the peaks are determined by the equation that is obtained from the equation determining the eigenmodes for the dielectric cylinder replacing the Hankel function of the first kind by the Neumann function. Similar features for the radiation generated by a charge moving along a helical orbit around/inside a dielectric cylinder have been discussed in [10]. This type of electron motion is employed in helical undulators.

Another type of the radiation that attracted a great deal of attention is the Smith-Purcell radiation (for reviews see [11, 12]). It arises when charged particles are in flight near a diffraction grating. The Smith-Purcell radiation presents a tunable source of the electromagnetic radiation over a wide range of frequency spectrum. It has a number of remarkable properties and is widely used in various fields of science and technology for the generation of electromagnetic radiation in different wavelength ranges and for the determination of the characteristics of emitting particles using the properties of the radiation field. In particular, the Smith-Purcell radiation is one of the basic mechanisms for the generation of electromagnetic waves in the millimeter and submillimeter wavelengths. The radiation having similar physical properties and induced by a charged particle in flight over a surface acoustic wave has been discussed in [13] (for a more general problem of the radiation from a charge intersecting a periodically deformed dynamical boundary between two media see [14]). The use of surface waves simplifies the control of the period and the amplitude of the periodic structure and, hence, the angular-frequency characteristics of the emitted radiation. Compared to the case of diffraction grating, the dynamical nature of the periodic structure leads to an additional shift in the radiation frequency for a given direction.

The previous investigations of the Smith-Purcell effect mainly consider the radiation sources moving along straight trajectories. In this case the radiation mechanism is purely Smith-Purcell one (possibly with an additional Cherenkov radiation if the source moves in a medium). In the present paper we consider a problem with two types of radiation mechanisms acting together: synchrotron and Smith-Purcell ones. Namely, we will study the radiation from a point charge rotating around a metallic diffraction grating on a cylindrical surface, with the strips parallel to the cylinder axis. Note that though the primary source of the radiation for both the synchrotron and Smith-Purcell emissions is the electromagnetic field of the charged particle, the Smith-Purcell radiation is formed by the medium as a result of its dynamic polarization by the field of the moving charge. The Smith-Purcell effect from an annular electron beam moving parallel to the axis of a cylindrical grating, with the grooves perpendicular to the axis, has been recently investigated in [15]. Of course, in this case the only radiation mechanism is the Smith-Purcell one.

The outline of the paper is the following. In the next section we consider the electromagnetic fields and the radiation from a charge rotating around a solid conducting cylinder. The surface charge and current densities, induced on the cylinder are determined. By using these densities, in section 3 we investigate the vector potential, the strengths of the electric and magnetic fields for a charge rotating around a cylindrical diffraction grating with metallic strips parallel to the cylinder axis. Then we evaluate the spectral-angular density of the radiation intensity and present the results of the numerical analysis for the number of the radiated quanta. The main results of the paper are summarized in section 4.

2 Radiation from a charge rotating around a conducting cylinder

In this section we consider the radiation of a point charge q , rotating with the velocity v along a circle of radius r_e around an infinitely long conducting cylinder with radius r_c , $r_c < r_e$ (see figure 1). For generality, we assume that the cylinder is immersed into a homogeneous medium with the dielectric permittivity ε . The corresponding electromagnetic field in the region outside the cylinder is investigated in [9] (for the radiation from a charge rotating inside a cylindrical waveguide with dielectric filling see [16]). In accordance with the problem symmetry, we use cylindrical coordinates (r, φ, z) with the axis z directed along the axis of the cylinder. For the cylindrical coordinates of the charge we shall take $(r, \varphi, z) = (r_e, \omega_0 t, 0)$, where $\omega_0 = v/r_e$ is the angular velocity of the rotation.

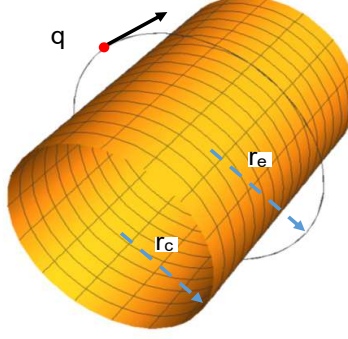


Figure 1: Geometry of the problem corresponding to a point charge q rotating around a conducting cylinder.

For the l th component of the vector potential one has the Fourier expansion

$$A_l(x) = \sum_{n=-\infty}^{+\infty} e^{in(\varphi - \omega_0 t)} \int_{-\infty}^{+\infty} dk_z e^{ik_z z} A_{nl}(k_z), \quad (1)$$

where $x = (t, r, \varphi, z)$ and $l = 1, 2, 3$ correspond to the r, φ, z components, respectively. In the region $r > r_c$, these components are decomposed as

$$A_{nl}(k_z) = A_{nl}^{(0)}(k_z) + A_{nl}^{(c)}(k_z), \quad (2)$$

where $A_{nl}^{(0)}(k_z)$ corresponds to the field in the absence of the cylinder and $A_{nl}^{(c)}(k_z)$ is the field induced by the presence of the cylinder. In the Lorentz gauge, for the separate contributions one has

$$\begin{aligned} A_{nl}^{(0)}(k_z) &= -\frac{vq}{4ci^{l-1}} \sum_{\alpha=\pm 1} \alpha^l J_{n+\alpha}(\lambda r_<) H_{n+\alpha}(\lambda r_>), \\ A_{nl}^{(c)}(k_z) &= \frac{vq}{4ci^{l-1}} \sum_{\alpha=\pm 1} \alpha^l \frac{H_{n+\alpha}(\lambda r_0)}{H_{n+\alpha}(\lambda r_1)} J_{n+\alpha}(\lambda r_1) H_{n+\alpha}(\lambda r), \end{aligned} \quad (3)$$

for $l = 1, 2$, and $A_{n3}^{(0)}(k_z) = A_{n3}^{(c)}(k_z) = 0$. Here, $J_\nu(x)$ and $H_\nu(x) \equiv H_\nu^{(1)}(x)$ are the Bessel function and the Hankel function of the first kind, $r_< = \min(r_e, r)$, $r_> = \max(r_e, r)$, and

$$\lambda = \sqrt{n^2 \omega_0^2 \varepsilon / c^2 - k_z^2}. \quad (4)$$

Having the vector potential we can evaluate the electric and magnetic fields. The corresponding Fourier expansions can be written in the form

$$F_l(x) = \sum_{n=-\infty}^{\infty} e^{in(\varphi-\omega_0 t)} \int_{-\infty}^{+\infty} dk_z e^{ik_z z} F_{nl}(k_z), \quad (5)$$

where $F = E$ and $F = H$ for the electric and magnetic fields, respectively. Considering the region $r > r_e$, for the Fourier components of the magnetic field with $n \geq 0$ one gets

$$\begin{aligned} H_{nl}(k_z) &= \frac{vqk_z}{4ci^{l-1}} \sum_{\alpha=\pm 1} \alpha^{l-1} B_{n+\alpha} H_{n+\alpha}(\lambda r), \quad l = 1, 2, \\ H_{n3}(k_z) &= \frac{ivq\lambda}{4c} \sum_{\alpha=\pm 1} \alpha B_{n+\alpha} H_n(\lambda r), \end{aligned} \quad (6)$$

with the notation

$$B_{n+\alpha} = J_{n+\alpha}(\lambda r_e) - \frac{H_{n+\alpha}(\lambda r_e)}{H_{n+\alpha}(\lambda r_c)} J_{n+\alpha}(\lambda r_c). \quad (7)$$

For the components with $n < 0$ we have the relation $H_{nl}(k_z) = H_{-nl}^*(-k_z)$. For $n \neq 0$, the electric field is found by using the relation $\mathbf{E}_n = ic(\varepsilon n \omega_0)^{-1} \text{rot } \mathbf{H}_n$. This leads to the expressions

$$\begin{aligned} E_{nl}(k_z) &= \frac{vq}{8i^l \varepsilon n \omega_0} \sum_{\alpha=\pm 1} \alpha^l [(n^2 \omega_0^2 \varepsilon / c^2 + k_z^2) B_{n+\alpha} - \lambda^2 B_{n-\alpha}] H_{n+\alpha}(\lambda r), \\ E_{n3}(k_z) &= \frac{vqk_z \lambda}{4\varepsilon n \omega_0} \sum_{\alpha=\pm 1} B_{n+\alpha} H_n(\lambda r), \end{aligned} \quad (8)$$

with $l = 1, 2$.

Similar to the vector potential, the Fourier components for the electric and magnetic fields are presented as

$$F_{nl}(k_z) = F_{nl}^{(0)}(k_z) + F_{nl}^{(c)}(k_z), \quad (9)$$

where $F_{nl}^{(0)}(k_z)$ are the corresponding components in the problem without the cylinder and the part $F_{nl}^{(c)}(k_z)$ is induced by the conducting cylinder. The expressions for $F_{nl}^{(0)}(k_z)$ are obtained from the formulae (6) and (8) by the replacement $B_{n+\alpha} \rightarrow J_{n+\alpha}(\lambda r_e)$. The contribution in the fields induced by the cylinder comes from the second term in the right-hand side of (7). The expressions for $F_{nl}^{(c)}(k_z)$ have the form (6) and (8) with the replacement $B_{n+\alpha} \rightarrow -J_{n+\alpha}(\lambda r_c) H_{n+\alpha}(\lambda r_e) / H_{n+\alpha}(\lambda r_c)$. In the region $r_c \leq r < r_e$ the expressions for the parts $F_{nl}^{(c)}(k_z)$ remain the same, whereas in the expressions for $F_{nl}^{(0)}(k_z)$ the replacements $J \rightleftharpoons H$ should be made. Comparing the expressions (3) for the parts $A_{nl}^{(0)}(k_z)$ and $A_{nl}^{(c)}(k_z)$, we see that for large values of n the Fourier component of the field induced by the cylinder in the region $r > r_e$ is approximated by the field of an effective point charge

$$q_{\text{im}} = -q \frac{r_e H_n(\lambda r_e)}{r_c H_n(\lambda r_c)}, \quad (10)$$

located on the cylinder surface and having cylindrical coordinates $(r, \varphi, z) = (r_c, \omega_0 t, 0)$.

If the charge is close to the cylinder surface, $r_e/r_c - 1 \ll 1$, for $B_{n+\alpha}$, to the leading order, one has

$$B_{n+\alpha} \approx -\frac{2i}{\pi \lambda r_c} \frac{r_e/r_c - 1}{H_{n+\alpha}(\lambda r_c)}. \quad (11)$$

This shows that in the limit $r_e \rightarrow r_c$ the fields in the region $r > r_e$ vanish. In this limit the field of the charge is compensated by its image.

Having the electric field in the region $r_c \leq r < r_e$ we can find the surface charge density $\sigma(\varphi, z, t)$ on the cylinder. For the corresponding Fourier transform, $\sigma_n(k_z)$, defined in accordance with

$$\sigma(\varphi, z, t) = \sum_{n=-\infty}^{+\infty} e^{in(\varphi-\omega_0 t)} \int_{-\infty}^{+\infty} dk_z e^{ik_z z} \sigma_n(k_z), \quad (12)$$

one has $\sigma_n = \varepsilon E_{n1, r=r_c}(k_z)/(4\pi)$. By using the expression for the radial component of the electric field it can be seen that

$$\sigma_n(k_z) = -\frac{qr_e}{8\pi^2 r_c^2} \sum_{\alpha=\pm 1} \frac{H_{n+\alpha}(\lambda r_e)}{H_{n+\alpha}(\lambda r_c)}. \quad (13)$$

Substituting into (12) and integrating over φ and z , we can show that

$$r_c \int_0^{2\pi} d\varphi \int_{-\infty}^{+\infty} dz \sigma(\varphi, z, t) = -q. \quad (14)$$

It is easy to see that, in the limit $r_e \rightarrow r_c$ for the surface charge (12) one gets $\sigma(\varphi, z, t)|_{r_e \rightarrow r_c} = -q\delta(\varphi - \omega_0 t)\delta(z)/r_c$, where we have assumed that $0 \leq \varphi - \omega_0 t < 2\pi$. The latter corresponds to a point charge $-q$ located on the cylinder surface.

For the surface current density induced on the cylinder surface one has $\mathbf{j}_s = c[\mathbf{n} \times \mathbf{H}]/(4\pi)|_{r=r_c}$, where \mathbf{n} is the normal to the cylinder. By using the expressions (6), we can see that the only nonzero component of the current density is along the azimuthal direction, $j_{sl} = 0$ for $l = 1, 3$, and $j_{s2} = -cH_{3, r=r_c}/(4\pi)$. From (6), for the corresponding Fourier component of the magnetic field one gets

$$H_{n3}(k_z)|_{r=r_c} = \frac{vq}{2\pi cr_c} \sum_{\alpha=\pm 1} \frac{H_{n+\alpha}(\lambda r_e)}{H_{n+\alpha}(\lambda r_c)}. \quad (15)$$

This shows that the Fourier components of the surface charge and current densities are related by the standard formula $j_{sn2}(k_z) = v'\sigma_n(k_z)$, where $v' = \omega_0 r_c = vr_c/r_e$ is the velocity of the charge image on the cylinder surface.

At large distances from the cylinder, the angular density of the radiation intensity at the frequency $n\omega_0$, $n = 1, 2, \dots$, is given by the expression

$$\frac{dI_n^{(c)}}{d\Omega} = \frac{q^2 n^2 \omega_0^2}{8\pi\sqrt{\varepsilon}c} \beta^2 \left[|B_{n+1} - B_{n-1}|^2 + |B_{n+1} + B_{n-1}|^2 \cos^2 \theta \right], \quad (16)$$

where $\beta = v\sqrt{\varepsilon}/c$, $d\Omega = \sin\theta d\theta d\varphi$ is the solid angle element, θ is the angle between the radiation direction and the axis z , and

$$k_z = \frac{n\omega_0}{c} \sqrt{\varepsilon} \cos \theta, \quad (17)$$

is the projection of the wave vector on the cylinder axis. For $B_{n\pm 1}$ in (16) one has the expression (7) with

$$\lambda = \frac{n\omega_0}{c} \sqrt{\varepsilon} \sin \theta, \quad (18)$$

and, hence, $\lambda r_e = n\beta \sin \theta$. Let us consider some limiting cases of the formula (16).

In the absence of the cylinder one has $B_{n+\alpha} = J_{n+\alpha}(\lambda r_e)$ and (16) is reduced to the corresponding expression for the synchrotron radiation in a homogeneous and isotropic medium (see [6]):

$$\frac{dI_n^{(0)}}{d\Omega} = \frac{q^2 n^2 \omega_0^2}{2\pi c \sqrt{\varepsilon}} \left[\beta^2 J_n'^2(n\beta \sin \theta) + \cot^2 \theta J_n^2(n\beta \sin \theta) \right]. \quad (19)$$

By using the asymptotic expression (11), in the limit $r_e \rightarrow r_c$ we see that the radiation intensity from a charge rotating around a conducting cylinder vanishes as $(r_e/r_c - 1)^2$. In this limit the field of the

charge is compensated by the field of its image on the cylinder surface. For small angles θ , to the leading order one gets

$$\frac{dI_n^{(c)}}{d\Omega} \approx \left[1 - (r_c/r_e)^{2(n-1)}\right]^2 \frac{dI_n^{(0)}}{d\Omega}, \quad (20)$$

with

$$\frac{dI_n^{(0)}}{d\Omega} \approx \frac{q^2 \omega_0^2}{\pi c \sqrt{\varepsilon}} \frac{(n\beta/2)^{2n}}{\Gamma^2(n)} \sin^{2(n-1)} \theta. \quad (21)$$

In a homogeneous medium, the only nonzero contribution to the radiation at the angle $\theta = 0$ comes from the harmonic $n = 1$. In the problem with the conducting cylinder, the radiation intensity at zero angle vanishes for all harmonics including $n = 1$.

For large values of the radiation harmonic n and for $x < 1$, we can use the asymptotic expressions

$$\begin{aligned} J_{n+\alpha}(nx) &\approx \frac{\eta_1^{1/2}(x)x^{-|\alpha|}}{\pi(1-x^2)^{1/4}} \left[K_{1/3}(n\eta_1(x)) - \alpha\sqrt{1-x^2}K_{2/3}(n\eta_1(x)) \right], \\ Y_{n+\alpha}(nx) &\approx -\frac{\eta_1^{1/2}(x)x^{-|\alpha|}}{(1-x^2)^{1/4}} \left[I_{1/3}^{(+)}(n\eta_1(x)) + \alpha\sqrt{1-x^2}I_{2/3}^{(+)}(n\eta_1(x)) \right], \end{aligned} \quad (22)$$

where $\alpha = 0, \pm 1$, $Y_\nu(u)$ is the Neumann function, $I_\nu^{(+)}(u) = I_\nu(u) + I_{-\nu}(u)$,

$$\eta_1(x) = \ln \frac{1 + \sqrt{1-x^2}}{x} - \sqrt{1-x^2}, \quad (23)$$

with $K_\nu(u)$ and $I_\nu(u)$ being the modified Bessel functions. For $x > 1$ the asymptotic formulas are given by

$$\begin{aligned} J_{n+\alpha}(nx) &\approx \frac{\eta_2^{1/2}(x)x^{-|\alpha|}}{\sqrt{3}(x^2-1)^{1/4}} \left[J_{1/3}^{(+)}(n\eta_2(x)) + \alpha\sqrt{x^2-1}J_{2/3}^{(-)}(n\eta_2(x)) \right], \\ Y_{n+\alpha}(nx) &\approx \frac{\eta_2^{1/2}(x)x^{-|\alpha|}}{(x^2-1)^{1/4}} \left[J_{1/3}^{(-)}(n\eta_2(x)) - \alpha\sqrt{x^2-1}J_{2/3}^{(+)}(n\eta_2(x)) \right], \end{aligned} \quad (24)$$

with $\alpha = 0, \pm 1$, $J_\nu^{(\pm)}(u) = J_\nu(u) \pm J_{-\nu}(u)$, and

$$\eta_2(x) = \sqrt{x^2-1} - \arccos(1/x). \quad (25)$$

The asymptotic formulas (22) and (24) are obtained from the uniform asymptotic expansions for the cylinder functions, given, for example, in [17], by using the expressions for the Airy functions and their derivatives in terms of the cylinder functions with the orders $\pm 1/3$ and $\pm 2/3$. Note that $\eta_j(1) = 0$ for $j = 1, 2$. The function $\eta_1(x)$ ($\eta_2(x)$) is a monotonically decreasing (increasing) function in the region $0 < x \leq 1$ ($1 \leq x < \infty$). For $|x-1| \ll 1$ one has

$$\eta_j(x) \approx \frac{2^{3/2}}{3}|x-1|^{3/2}. \quad (26)$$

The asymptotic expressions for the Hankel function are obtained from (22) and (24), by taking into account that $H_\nu(x) = J_\nu(x) + iY_\nu(x)$.

For $\beta \sin \theta < 1$, the radiation from a charge rotating in a homogeneous medium is emitted on the harmonics $n \lesssim 1/\eta_1(\beta \sin \theta)$. For $n \gg 1/\eta_1(\beta \sin \theta)$ the corresponding radiation intensity is suppressed by the factor $e^{-2n\eta_1(\beta \sin \theta)}$. Under the condition $\beta > 1$ and for $\beta \sin \theta > 1$, by using the asymptotic expressions (24), one gets

$$\frac{dI_n^{(0)}}{d\Omega} \approx \frac{q^2 n^2 \omega_0^2}{6\pi c \sqrt{\varepsilon}} \frac{\eta_2(y)}{\sin^2 \theta} \left[(y^2-1)^{1/2} J_{2/3}^{(-)2}(n\eta_2(y)) + \cos^2 \theta \frac{J_{1/3}^{(+)}(n\eta_2(y))}{(y^2-1)^{1/2}} \right], \quad (27)$$

with $y = \beta \sin \theta$. In this case the radiation intensity increases with increasing n . However, for large values of n the dispersion of the dielectric permittivity should be taken into account, $\varepsilon = \varepsilon(n\omega_0)$, and the increase of the intensity is restricted by the Cherenkov condition $v\varepsilon(n\omega_0)/c > 1$.

For a charge rotating around a conducting cylinder and under the condition $\beta \sin \theta < 1$, the cylinder-induced effects in the radiation intensity on the harmonics $n \gg 1/\eta_1(\beta \sin \theta)$, compared with $dI_n^{(0)}/d\Omega$, are suppressed by an additional factor $e^{-2n[\eta_1(\beta' \sin \theta) - \eta_1(\beta \sin \theta)]}$. Note that for the ratio r_c/r_e close to 1 one has

$$\eta_1(\beta' \sin \theta) - \eta_1(\beta \sin \theta) \approx \sqrt{1 - \beta^2 \sin^2 \theta} (1 - r_c/r_e). \quad (28)$$

In this case the relative suppression factor can be presented as

$$e^{-2n[\eta_1(\beta' \sin \theta) - \eta_1(\beta \sin \theta)]} \approx \exp[-4\pi \sqrt{\beta^{-2} - \sin^2 \theta} (r_e - r_c)/\lambda_r], \quad (29)$$

where λ_r is the radiation wavelength. For the radiation in the vacuum ($\varepsilon = 1$) and for the radiation angles θ not too close to $\pi/2$, the effects induced by the cylinder are exponentially suppressed for wavelengths $\lambda_r < r_e - r_c$. For relativistic particles and for angles close to $\pi/2$ one has $\beta^{-2} - \sin^2 \theta \approx \gamma^{-2} + (\theta - \pi/2)^2$ and the contribution of the cylinder to the total radiation intensity can be essential for wavelengths much smaller than the distance from the cylinder.

In the figures below we plot the angular density for the number of the quanta on a given harmonic radiated per period of the charge rotation:

$$\frac{dN_n^{(c)}}{d\Omega} = \frac{T}{\hbar n \omega_0} \frac{dI_n^{(c)}}{d\Omega}. \quad (30)$$

Figure 2 presents this quantity as a function of the angle θ (in radians) for the harmonic $n = 25$ and for the electron energy $E_e = 2$ MeV. The numbers near the curves are the values of the ratio r_c/r_e . The dashed curves correspond to the radiation in the absence of a conducting cylinder. The panels (a) and (b) present the cases $\varepsilon = 1$ (radiation in the vacuum) and $\varepsilon = 3.75$ (dielectric permittivity for quartz). As is seen, in the second case the number of the radiated quanta is essentially larger compared with the case of the radiation in the vacuum. This is related to the fact that, in addition to the synchrotron radiation, one has also Cherenkov radiation. For the case of the panel (b), the radiation is mainly located in the angular region $\pi/2 - \theta_C < \theta < \pi/2 + \theta_C$, where $\theta_C = \arccos(1/\beta)$. For the parameters corresponding to this panel one has $\pi/2 - \theta_C \approx 0.56$, whereas for the left peak one has $\theta \approx 0.61$. The number of oscillations in the angular range $\pi/2 - \theta_C < \theta < \pi/2 + \theta_C$ increases with increasing n . For the case of the radiation in the vacuum, the number of the radiated quanta is decreasing with increasing r_c/r_e . As it has been already explained above, the radiation intensity vanishes in the limit $r_c/r_e \rightarrow 1$.

Figure 3 presents the number of the radiated quanta as a function of the harmonic n for the case of the radiation in the vacuum ($\varepsilon = 1$). The graphs are plotted for $r_c/r_e = 0.9$. The numbers near the curves are the corresponding values of the angle θ and the numbers in the brackets correspond to the value of the energy in MeVs. We have considered the radiation in the plane of the radiation ($\theta = \pi/2$) and along the angles at which the angular density for the number of the radiated quanta has a maximum for the harmonic $n = 25$.

3 Electromagnetic fields and radiation intensity in the geometry of a cylindrical grating

In this section we consider the radiation from a charge rotating around a diffraction grating on the cylindrical surface with radius r_c . The grating consists infinitely long metallic strips with width a and with the separation b (see figure 4). The problem is mathematically complicated and an exact

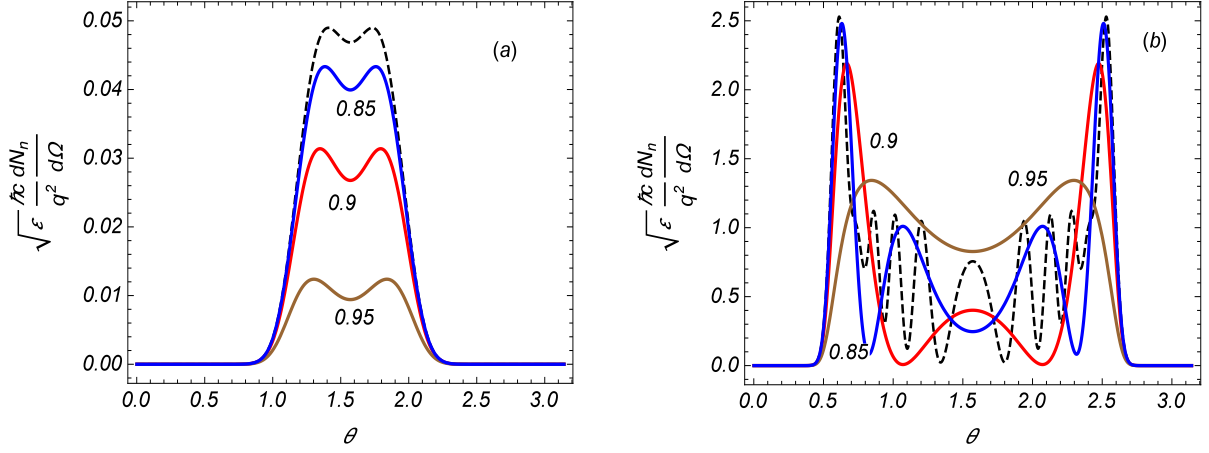


Figure 2: Angular density of the number of the radiated quanta per period of the charge rotation versus the radiation angle with respect to the cylinder axis. The graphs are plotted for the electron energy 2 MeV and for the radiation harmonic $n = 25$. The numbers near the curves are the values of r_c/r_e and the dashed curves correspond to the radiation in the absence of the cylinder. For the panels (a) and (b) we have taken $\varepsilon = 1$ and $\varepsilon = 3.75$, respectively.

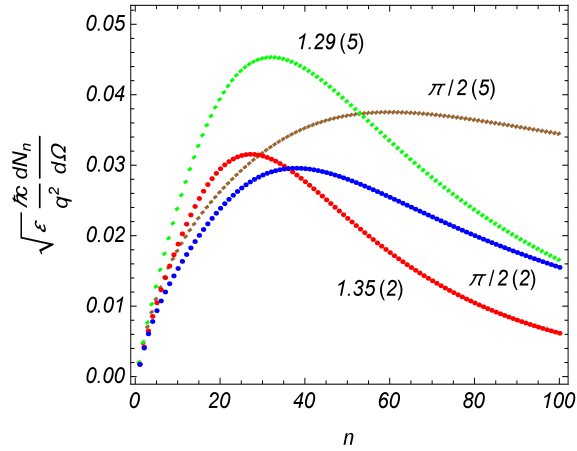


Figure 3: Angular density of the number of the radiated quanta as a function of the radiation harmonic for the energies of the electron 2 MeV and 5 MeV (numbers in the brackets) and for $r_c/r_e = 0.9$, $\varepsilon = 1$. The numbers near the curves correspond to the values of θ .

analytical result is not available. This is already the case for simpler problems of the Smith-Purcell radiation from planar gratings. For the latter geometry various approximate analytic and numerical methods have been developed for the evaluation of the spectral-angular distribution of the radiation intensity (for the comparison of different models in the calculations of the Smith-Purcell radiation intensity see [18]). On the base of the analysis given above, we approximate the effect of the grating on the radiation intensity by the surface currents induced on the strips by the field of the rotating charge. For planar gratings this method has been discussed in [19, 20] (for further developments of the method see [21]).

For the current density induced on the strips of the cylindrical grating one has

$$j_l^{(s)} = v_l' \sigma^{(s)}(\varphi, z, t) \delta(r - r_c), \quad (31)$$

where $v_l' = v' \delta_{2l}$. For the surface charge density we use the expression

$$\sigma^{(s)}(\varphi, z, t) = \begin{cases} \sigma(\varphi, z, t), & m\varphi_1 \leq \varphi \leq m\varphi_1 + \varphi_0 \\ 0, & \text{otherwise} \end{cases}, \quad (32)$$

where $m = 0, 1, 2, \dots, N - 1$, with

$$N = \frac{2\pi r_c}{a + b}, \quad (33)$$

being the number of the periods of the grating. In (32), the function $\sigma(\varphi, z, t)$ is given by (12) with $\sigma_n(k_z)$ from (13) and

$$\varphi_0 = a/r_c, \quad \varphi_1 = (a + b)/r_c, \quad (34)$$

are the angular width of the strips and the angular period of the grating, respectively.

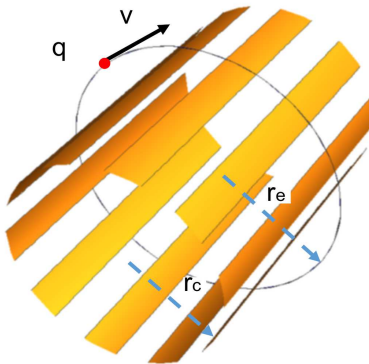


Figure 4: Point charge rotating around a cylindrical grating.

3.1 Electric and magnetic fields

The vector potential for the field generated by the surface current density (31) is determined from the formula

$$A_i^{(s)}(\mathbf{r}, t) = -\frac{1}{2\pi^2 c} \int G_{il}(\mathbf{r}, t, \mathbf{r}', t') j_l^{(s)}(\mathbf{r}', t') d\mathbf{r}' dt', \quad (35)$$

where $G_{il}(\mathbf{r}, t, \mathbf{r}', t')$ is the electromagnetic field Green function in a homogeneous medium with permittivity ε and summation over l is understood. In accordance with the problem symmetry, for the

Green function we have the following Fourier expansion:

$$G_{il}(\mathbf{r}, t, \mathbf{r}', t') = \sum_{n=-\infty}^{+\infty} \int_{-\infty}^{+\infty} dk_z \int_{-\infty}^{+\infty} d\omega G_{il}(n, k_z, \omega, r, r') e^{in(\varphi-\varphi') + ik_z(z-z') - i\omega(t-t')}. \quad (36)$$

Substituting in (35) and by taking into account (31), after redefining $n \rightarrow n + Nm$, one gets

$$\begin{aligned} A_l^{(s)}(\mathbf{r}, t) &= -\frac{4\pi v' r_c}{c} \sum_{n,m=-\infty}^{+\infty} e^{-iNm\varphi_0/2} S_m e^{i(n-Nm)\varphi - in\omega_0 t} \\ &\times \int_{-\infty}^{+\infty} dk_z e^{ik_z z} G_{l2}(n + Nm, k_z, n\omega_0, r, r_c) \sigma_n(k_z), \end{aligned} \quad (37)$$

with the notation

$$S_m = \frac{1}{\pi m} \sin\left(\frac{\pi m a}{a+b}\right). \quad (38)$$

For the Fourier components of the Green tensor, appearing in (37), one has

$$G_{l2}(n + Nm, k_z, n\omega_0, r, r_c) = \frac{\pi}{4} i^{1-l} \sum_{\alpha=\pm 1} \alpha^l J_{n+Nm+\alpha}(\lambda r'_<) H_{n+Nm+\alpha}(\lambda r'_>), \quad (39)$$

for $l = 1, 2$ and $G_{32}(n, k_z, \omega, r, r_c) = 0$. Here, λ is defined by (4) and $r'_< = \min(r_c, r)$, $r'_> = \max(r_c, r)$. Substituting (39) into (37), the components of the vector potential are presented as the Fourier expansion

$$A_l^{(s)}(x) = \sum_{n,m=-\infty}^{+\infty} \int_{-\infty}^{+\infty} dk_z e^{i(n+mN)\varphi - in\omega_0 t + ik_z z} A_{nml}^{(s)}(k_z, r), \quad (40)$$

where

$$A_{nml}^{(s)}(k_z, r) = \frac{i^{1-l} qv}{4c} e^{-iNm\varphi_0/2} S_m \sum_{\alpha=\pm 1} \alpha^l \frac{H_{n+\alpha}(\lambda r_c)}{H_{n+\alpha}(\lambda r_c)} J_{n+mN+\alpha}(\lambda r'_<) H_{n+mN+\alpha}(\lambda r'_>), \quad (41)$$

for $l = 1, 2$ and $A_{nm3}^{(s)}(k_z, r) = 0$. Compared to the case of a solid cylinder, the Fourier expansion for the geometry of a grating contains an additional summation over m . The latter corresponds to the periodic structure along the azimuthal direction. As a result, the vector potential for the total field is presented as

$$A_l(x) = A_l^{(0)}(x) + A_l^{(s)}(x), \quad (42)$$

where $A_l^{(0)}(x)$ is the corresponding field in a homogeneous medium with permittivity ε .

The expansions similar to (40) can be written for the field strengths:

$$F_l^{(s)}(x) = \sum_{n,m=-\infty}^{+\infty} \int_{-\infty}^{+\infty} dk_z e^{i(n+mN)\varphi - in\omega_0 t + ik_z z} F_{nml}^{(s)}(k_z, r), \quad (43)$$

with $F = E$ and $F = H$ for the electric and magnetic fields, respectively. For the Fourier components of the magnetic field in the region $r > r_c$ one gets

$$\begin{aligned} H_{nml}^{(s)}(k_z, r) &= \frac{qv k_z}{4c i^{l-1}} \sum_{\alpha=\pm 1} \alpha^{l-1} B_{n,m}^{(\alpha)} H_{n+mN+\alpha}(\lambda r), \\ H_{nm3}^{(s)}(k_z, r) &= \frac{iqv \lambda}{4c} \sum_{\alpha=\pm 1} \alpha B_{n,m}^{(\alpha)} H_{n+mN}(\lambda r). \end{aligned} \quad (44)$$

with $l = 1, 2$ and with the notation

$$B_{n,m}^{(\alpha)} = -e^{-\frac{\pi ia}{a+b}m} S_m \frac{H_{n+\alpha}(\lambda r_e)}{H_{n+\alpha}(\lambda r_c)} J_{n+mN+\alpha}(\lambda r_c). \quad (45)$$

For $n \neq 0$, the spectral components of the electric field are found from $\mathbf{E}_n = ic(\varepsilon n \omega_0)^{-1} \text{rot } \mathbf{H}_n$. For the Fourier components, this gives the expressions

$$\begin{aligned} E_{nml}^{(s)}(k_z, r) &= \frac{i^{-l} qv}{8\varepsilon n \omega_0} \sum_{\alpha=\pm 1} \alpha^l \left[(n^2 \omega_0^2 \varepsilon / c^2 + k_z^2) B_{n,m}^{(\alpha)} - \lambda^2 B_{n,m}^{(-\alpha)} \right] H_{n+mN+\alpha}(\lambda r), \\ E_{nm3}^{(s)}(k_z, r) &= \frac{qv k_z \lambda}{4\varepsilon n \omega_0} \sum_{\alpha=\pm 1} B_{n,m}^{(\alpha)} H_{n+mN}(\lambda r), \end{aligned} \quad (46)$$

where $l = 1, 2$.

We can write the expansion of the type (43) for the total fields

$$F_l(x) = F_l^{(0)}(x) + F_l^{(s)}(x). \quad (47)$$

In the region $r > r_e$, the expressions for the corresponding Fourier components are obtained from (44) and (46) by the replacement $B_{n,m}^{(\alpha)} \rightarrow D_{n,m}^{(\alpha)}$ with

$$D_{n,m}^{(\alpha)} = \delta_{0m} J_{n+\alpha}(\lambda r_e) + B_{n,m}^{(\alpha)}. \quad (48)$$

Here the first term in the right-hand side comes from the part of the field corresponding to the problem with a homogeneous medium when the cylindrical grating is absent. In the region $r_c < r < r_e$, the expressions for $F_l^{(s)}(x)$ remain the same, whereas in the expressions for the part $F_l^{(0)}(x)$ the replacement $J \rightleftharpoons H$ of the Bessel and Hankel functions should be made.

3.2 Radiation intensity

Having the fields, we can evaluate the radiation intensity from a charge rotating around a diffraction grating. The average energy flux per unit time through the cylindrical surface of radius r , coaxial with the axis of the grating, is given by

$$I^{(g)} = \frac{c}{4\pi T} \int_0^{2\pi} d\varphi \int_0^T dt \int_{-\infty}^{\infty} dz r \mathbf{n}_r \cdot [\mathbf{E} \times \mathbf{H}], \quad (49)$$

where $T = 2\pi/\omega_0$ and \mathbf{n}_r is the unit vector along the radial direction r . Substituting the Fourier expansions of the type (43) for the electric and magnetic fields, we obtain the following representation

$$I^{(g)} = \pi c r \sum_{n,m=-\infty}^{+\infty} \int_{-\infty}^{+\infty} dk_z [E_{nm2}(k_z, r) H_{nm3}^*(k_z, r) - E_{nm3}(k_z, r) H_{nm2}^*(k_z, r)], \quad (50)$$

where the Fourier components are given by the expressions obtained from (44) and (46) with the replacement $B_{n,m}^{(\alpha)} \rightarrow D_{n,m}^{(\alpha)}$.

For large values of r , by using the asymptotic expressions for the Hankel function for large arguments, we see that for the radiation field $\lambda^2 > 0$ that corresponds to the integration region $k_z^2 < n^2 \omega_0^2 \sqrt{\varepsilon}/c^2$. In this region, introducing a new integration variable θ in accordance with (17), the radiation intensity is presented in the form

$$I^{(g)} = 2\pi \sum_{n=1}^{\infty} \int_0^{\pi} d\theta \sin \theta \frac{dI_n^{(g)}}{d\Omega}, \quad (51)$$

with the angular density of the radiation intensity at a given harmonic $n\omega_0$:

$$\frac{dI_n^{(g)}}{d\Omega} = \frac{q^2\beta^2 n^2 \omega_0^2}{8\pi c\sqrt{\varepsilon}} \sum_{m=-\infty}^{+\infty} \left[\left| R_{n,m}^{(+1)} - R_{n,m}^{(-1)} \right|^2 + \cos^2\theta \left| R_{n,m}^{(+1)} + R_{n,m}^{(-1)} \right|^2 \right]. \quad (52)$$

Here, as before, θ is the angle between the radiation direction and the axis z , and

$$R_{n,m}^{(\alpha)} = \delta_{0m} J_{n+\alpha}(n\beta \sin\theta) - S_m \frac{H_{n+\alpha}(n\beta \sin\theta)}{H_{n+\alpha}(n\beta' \sin\theta)} J_{n+mN+\alpha}(n\beta' \sin\theta), \quad (53)$$

with $\beta' = r_c\beta/r_e$. Note that $R_{n,m}^{(\alpha)} = e^{-\frac{i\pi m}{1+b/a}} D_{n,m}^{(\alpha)}$. The part in the radiation intensity coming from the first term in the right-hand side of (53) corresponds to the radiation in a homogeneous medium. The remaining parts are induced by the diffraction grating.

For $a = 0$ one has $S_m = 0$ and (52) is reduced to $dI_n^{(0)}/d\Omega$, given by (19). Another special case $b = 0$ corresponds to a conducting cylinder. In this case, by taking into account that $S_m = \delta_{0m}$, we see that $D_{n,m}^{(\alpha)} = \delta_{0m} B_n^{(\alpha)}$ and the radiation intensity (52) coincides with (16). If the charge trajectory is close to the grating, to the leading order, in (53) we can put $\beta' = \beta$ and the radiation intensity is simplified to

$$\begin{aligned} \left. \frac{dI_n^{(g)}}{d\Omega} \right|_{r_1=r_0} &= \left(\frac{b}{a+b} \right)^2 \frac{dI_n^{(0)}}{d\Omega} + \frac{q^2 n^2 \omega_0^2}{2\pi c\sqrt{\varepsilon}} \sum_{m \neq 0} S_m^2 \\ &\times \left[\beta^2 J_{n+mN}^2(n\beta \sin\theta) + \cot^2\theta (1 + mN/n)^2 J_{n+mN}^2(n\beta \sin\theta) \right]. \end{aligned} \quad (54)$$

As it has been mentioned above, under the condition $\beta \sin\theta < 1$, for a given direction θ of the radiation and for the harmonics $n \gg \eta_1(\beta \sin\theta)$, the first term in the right-hand side of (54) is suppressed by the factor $e^{-2n\eta_1(\beta \sin\theta)}$. This may not be the case for the second term corresponding to the contribution of the Smith-Purcell radiation. Indeed, mathematically, the smallness of the part $dI_n^{(0)}/d\Omega$ is related to the fact that under the specified conditions the Bessel function $J_n(n\beta \sin\theta)$ is exponentially small. The Smith-Purcell part of the radiation contains the Bessel functions with the orders $n + mN$. Under the condition $|n + mN| \ll n\beta \sin\theta$ one has $J_{n+mN}(n\beta \sin\theta) \sim 1/\sqrt{n}$ and the corresponding contributions to (54) are not small.

As it has been mentioned in the previous section, for a charge rotating in homogeneous medium or for a charge rotating around a conducting cylinder, the angular density of the radiation intensity for the harmonics with $n > 1$ vanishes in the limit $\theta \rightarrow 0$. This may not be the case in the presence of the diffraction grating. For example, if $N > 2$ and $(n \pm 1)/N$ is an integer (note that only one of this numbers can be an integer), then for small angles the dominant contribution to (52) comes from the term with $m = -(n \pm 1)/N$ and to the leading order one has

$$\frac{dI_n^{(g)}}{d\Omega} \approx \frac{q^2\beta^2 n^2 \omega_0^2}{4\pi\sqrt{\varepsilon}c} S_{(n\pm 1)/N}^2 (r_1/r_0)^{2n\pm 2}. \quad (55)$$

The corresponding radiation intensity in a homogeneous medium vanishes as $\sin^{2n-2}(\theta)$ (see (21)).

In the geometry of diffraction grating the behavior of the radiation intensity on large values of the harmonic n can be essentially different from that for a charge rotating in the vacuum or around a solid cylinder. As an illustration let us consider the charge rotating in the vacuum ($\varepsilon = 1$) around the grating. In this case one has $\beta \sin\theta < 1$ and for large values of n for the cylinder functions in (53) with the orders $n + \alpha$ we can use the asymptotic formulas (22). In particular, for the harmonics $n \gg 1/\eta_1(\beta \sin\theta)$ the part corresponding to the pure synchrotron radiation (coming from the first term in the right-hand side of (53)) is suppressed by the factor $e^{-2n\eta_1(\beta \sin\theta)}$. This may not be the case for the Smith-Purcell part in the radiation intensity, coming from the last term in (53). Indeed,

for values of m for which the order $n + mN + \alpha$ of the Bessel function is not large by the modulus, one has $J_{n+mN+\alpha}(n\beta' \sin \theta) \sim 1/\sqrt{n}$ and for the radius of the circular orbit sufficiently close to the radius of the grating (in order to escape the exponential suppression coming from the ratio of the Hankel functions in (53)), under the condition $\eta(\beta' \sin \theta)/\eta(\beta \sin \theta) - 1 \ll 1$, the Smith-Purcell part in the radiation intensity dominates. By taking into account (28), this condition can be written as

$$1 - \frac{r_c}{r_e} \ll \frac{\eta_1(\beta \sin \theta)}{\sqrt{1 - \beta^2 \sin^2 \theta}}. \quad (56)$$

For the ratio of the Hankel functions in (53) one has

$$\frac{H_{n+\alpha}(n\beta \sin \theta)}{H_{n+\alpha}(n\beta' \sin \theta)} \approx \frac{r_c}{r_e} \frac{(1 - y'^2)^{1/4}}{(1 - y^2)^{1/4}} \frac{1 + \alpha\sqrt{1 - y'^2}}{1 + \alpha\sqrt{1 - y^2}} e^{-n[\eta_1(y') - \eta_1(y)]}, \quad (57)$$

with $y = \beta \sin \theta$ and $y' = \beta' \sin \theta$. Under the condition $n \gg 1/\eta_1(\beta \sin \theta)$ the Smith-Purcell contribution to the radiation intensity contains the factor (29). As a consequence, the values for the corresponding radiation harmonics are restricted by the condition

$$n\sqrt{1 - \beta^2 \sin^2 \theta}(1 - r_c/r_e) \lesssim 1. \quad (58)$$

Note that for $1 - \beta \sin \theta \ll 1$ the condition (56) is simplified to $1 - r_c/r_e \ll 1 - \beta \sin \theta$.

3.3 Numerical illustrations

For the further clarification of the radiation properties here we consider numerical examples. Similar to the case of a metallic cylinder, we present the results of the numerical investigations for the angular density of the number of the radiated quanta per period of rotation,

$$\frac{dN_n^{(g)}}{d\Omega} = \frac{T}{\hbar n \omega_0} \frac{dI_n^{(g)}}{d\Omega}. \quad (59)$$

In figure 5, for the electron with the energy 2 MeV, we have plotted this quantity for the harmonic

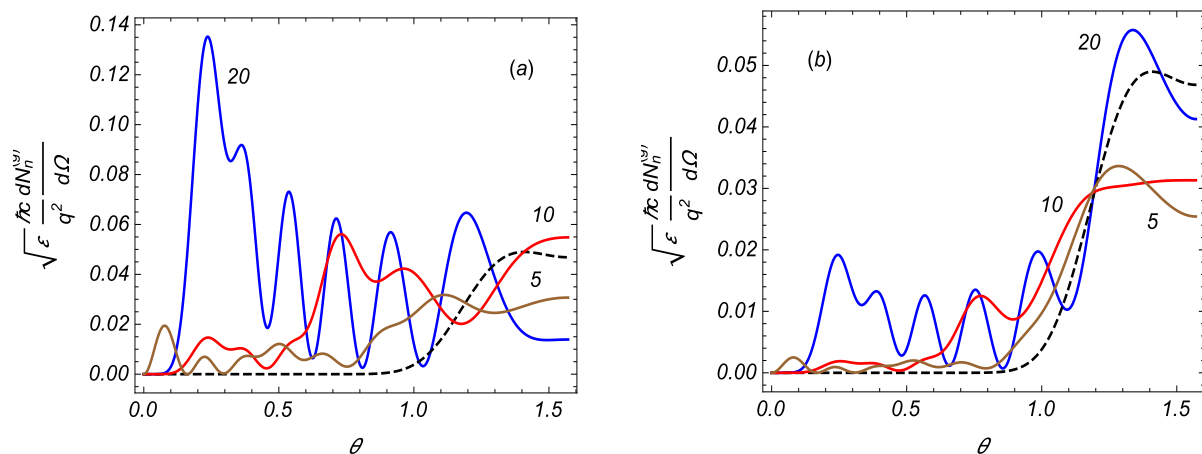


Figure 5: The angular dependence of the number of the radiated quanta per period of the charge rotation for the electron energy 2 MeV and for the radiation harmonic $n = 25$. The numbers near the curves are the values of N . The panels (a) and (b) correspond to $r_c/r_e = 0.99$ and $r_c/r_e = 0.95$, respectively. For the other parameters we have taken $b/a = 1$ and $\varepsilon = 1$.

$n = 25$ as a function of the angle θ (in radians) for different values of the parameter N (the numbers near the curves). The corresponding graphs in the region $\pi/2 \leq \theta \leq \pi$ are symmetric to the ones presented in figure 5 with respect to $\theta = \pi/2$. For the parameters of the grating we have taken $b/a = 1$ and $\varepsilon = 1$. The panel (a) corresponds to $r_c/r_e = 0.99$ and for the panel (b) $r_c/r_e = 0.95$. The dashed curves correspond to the radiation in the absence of the grating. As is seen, for the angles not close to the rotation plane, the radiation intensity is dominated by the Smith-Purcell part. For these angles one has the suppression of the radiation with decreasing values of the ratio r_c/r_e . Note that $\sqrt{\varepsilon} dN_n^{(g)}/d\Omega$ depends on the parameters ε , v , r_e , r_c in the form of the combinations β and r_e/r_c . The parameters of the diffraction grating enter through the factor S_m from (38) and through the number of periods N appearing in the index of the Bessel function in (53). Note that the radiation wavelength is given by the relation $\lambda_r = 2\pi r_e/(n\beta)$.

The same as in figure 5, for the energy of the electron 1 MeV, is plotted in figure 6. These graphs

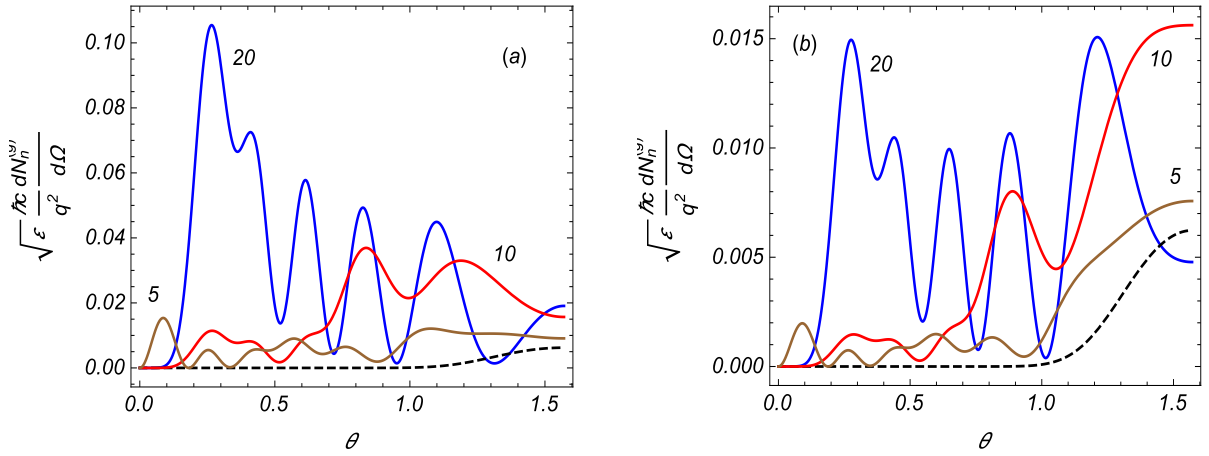


Figure 6: The same as in figure 5 for the energy of the electron 1 MeV.

show that, with decreasing energy, the relative contribution of the synchrotron radiation decreases and the Smith-Purcell part is dominant. In accordance with the explanation given above, for large values of n and N the main contribution to the radiation intensity comes from the term with the lowest value for $|n + mN + \alpha|$. In particular, for the examples with $n = 25$, $N = 20$ we have numerically checked that the dominant contribution in (52) comes from the term in the series over m with $m = -1$. The locations of the local maxima and minima of the radiation intensity are approximately determined by the local maxima and by the locations of the zeros for the Bessel function $J_{n-N-1}^2(n\beta' \sin \theta)$.

As it has been noted before, for a given harmonic n , the most strong radiation at small angles θ is obtained for the number of periods $N = n \pm 1$. This feature is illustrated in figure 7, where the angular dependence of the number of the radiated quanta is displayed for $r_c/r_e = 0.95, 0.97, 0.99$. The curves with increasing values for $dN_n^{(g)}/d\Omega|_{\theta=0}$ correspond to increasing values of r_c/r_e . The panels (a) and (b) are plotted for $n = 25$, $N = 24$ and $n = 15$, $N = 14$, respectively. The graphs for $N = 26$ and $N = 16$ have the structure similar to the ones in panels (a) and (b), respectively. Again, we have checked that for angles $\theta < 1$ rad the contribution of the term $m = -1$ is dominated in the radiation intensity and the oscillatory behavior comes from the function $J_{n-N-1}^2(n\beta' \sin \theta)$. The results depicted in figure 7 show that, for given characteristics of the charge (energy, radius of the orbit), by the choice of the parameters for the diffraction grating, one can have highly directional radiation on a given harmonic n directed near the normal to the plane of the charge rotation.

It is also of interest to see the dependence of the radiation characteristics on the ratio b/a and on the energy of the radiating charge. In figure 8, for the electron with the energy 2 MeV, we present the angular density of the number of the radiated quanta on the harmonic $n = 25$ versus the angle θ and

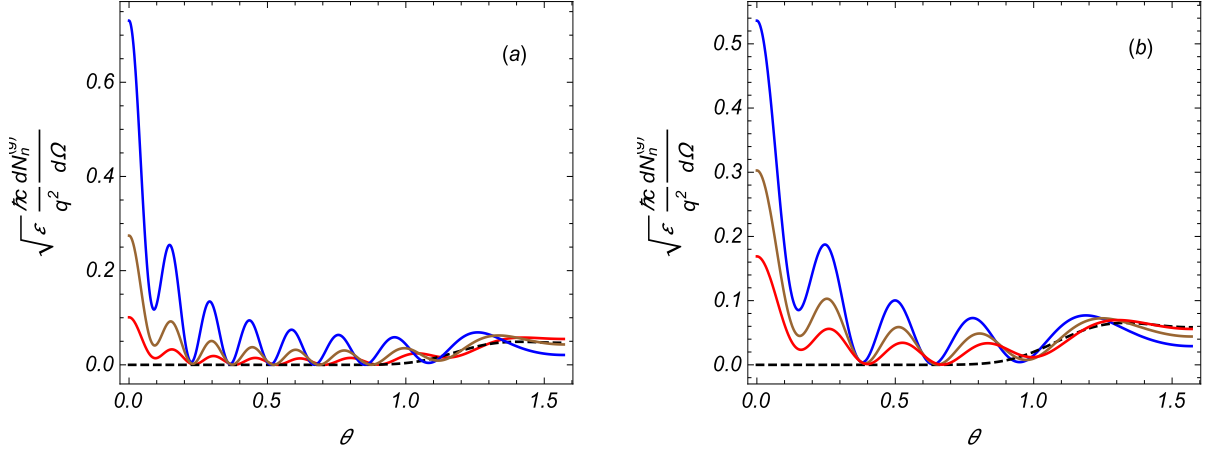


Figure 7: The angular density of the number of the radiated quanta as a function of θ for the electron energy 2 MeV and for $r_c/r_e = 0.95, 0.97, 0.99$ (upper curves near $\theta = 0$ correspond to larger values of r_c/r_e). The panels (a) and (b) are plotted for $n = 25, N = 24$ and $n = 15, N = 14$, respectively.

the parameter b/a (left panel) and versus θ and $\gamma = E_e/(m_e c^2)$ for $b/a = 1$ (right panel), with E_e being the energy of the electron. For the other parameters we have taken the values $N = 28, r_c/r_e = 0.99, \varepsilon = 1$. In the limit $b/a \ll 1$ we recover the result for a charge rotating around a conducting cylinder. In the opposite limit $b/a \gg 1$ the result for the rotation in the vacuum is obtained. As is seen, for the example considered in figure 8, the locations of the angular peaks are not sensitive to the ratio b/a . As a function of b/a , the radiation intensity takes its maximum value for b/a close to 1. From the right panel of figure 8 we see that, for $\gamma \gtrsim 3$ and for the angles θ not too close to $\pi/2$ (rotation plane), the heights and the locations of the angular peaks in the radiation intensity are not sensitive to the value of the electron energy E_e .

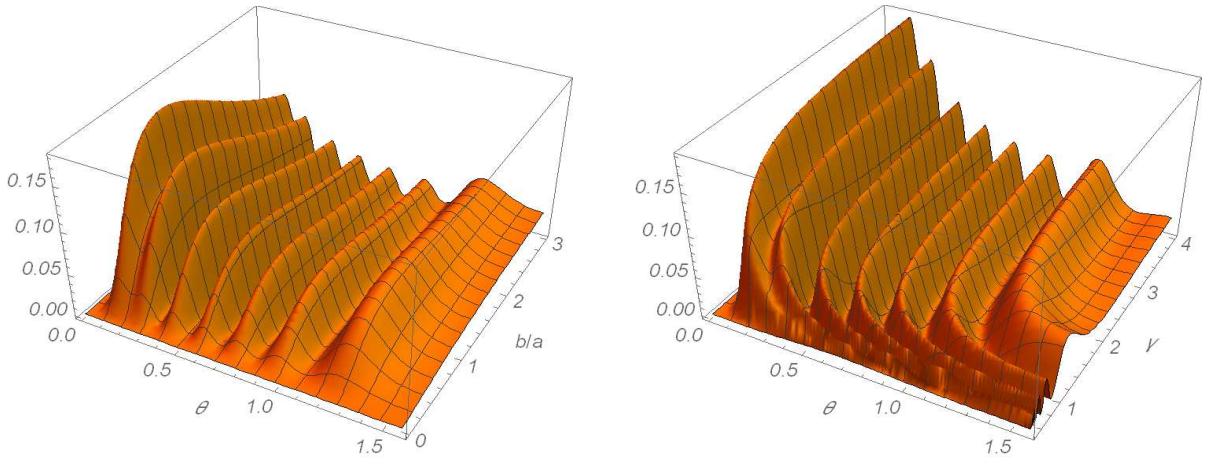


Figure 8: Number of the radiated quanta on the harmonic $n = 25$ versus θ and the ratio b/a for the electron with the energy 2 MeV (left panel) and versus θ and the gamma factor for $b/a = 1$ (right panel). For the values of the other parameters we have taken $N = 28, r_c/r_e = 0.99, \varepsilon = 1$.

In order to see the dependence on the number of the radiation harmonic, in figure 9 we have displayed the number of the radiated quanta as a function of n for the electron of the energy 2 MeV. The panels (a) and (b) are plotted for $N = 20, \theta = 0.24$ and $N = 24, \theta = 0.15$. These values of the

angle correspond to the local peaks in the angular distribution for the examples presented in figures 7 and 8. For these angles the radiation is mainly dominated by the Smith-Purcell part. The synchrotron part of the radiation is mainly located near the angle $\theta = \pi/2$. The corresponding radiation intensity, $dI_n^{(0)}/d\Omega$, increases with increasing n up to the values $n_{\max} \approx \gamma^3$. For the energy corresponding to figure 9 one has $n_{\max} \approx 60$. As regards the angular density of the number of the radiated quanta, $dN_n^{(0)}/d\Omega$, it monotonically decreases with increasing n .

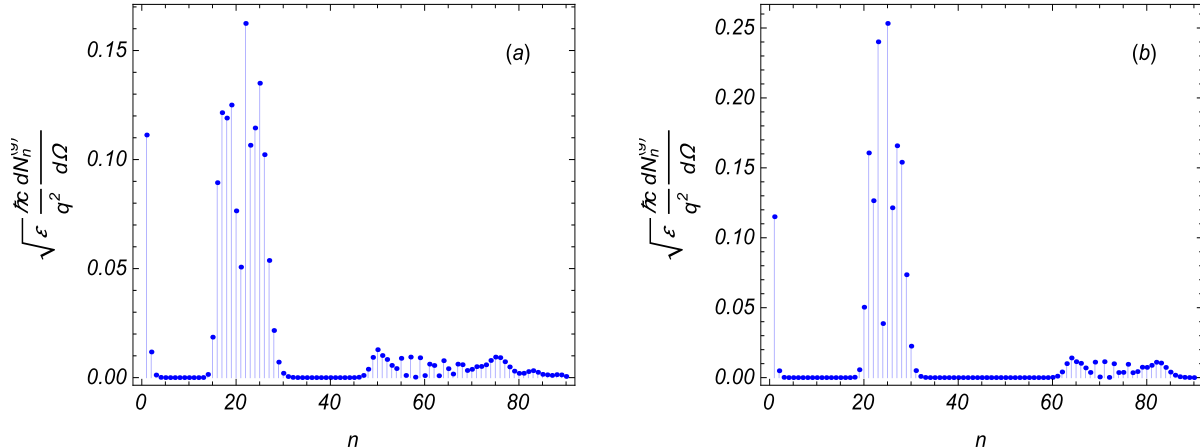


Figure 9: The angular density of the number of the radiated quanta as a function of the radiation harmonic for the electron energy 2 MeV and for $r_c/r_e = 0.99$. For the panels (a) and (b) one has $N = 20$, $\theta = 0.24$ and $N = 24$, $\theta = 0.15$, respectively.

4 Summary

We have investigated the radiation from a charge rotating around conductors with cylindrical symmetry. First the problem is considered with a charge rotating around a conducting cylinder immersed in a homogeneous and isotropic medium. The Fourier components of the electromagnetic fields, defined in accordance with (5), are decomposed into the parts corresponding to a charge rotating in a homogeneous medium, in the absence of the cylinder, and into the parts induced by the presence of the cylinder (see (9)). The Fourier components of the total fields are given by the expressions (6) and (8) with the coefficients defined in (7). The expressions for the cylinder induced parts are obtained from (6) and (8) replacing $B_{n+\alpha}$ by the second term in the right-hand side of (7). Having the fields, we have evaluated the surface charge and current densities induced by the field of the charge on the cylinder surface. For the Fourier component of the surface charge density one has the expression (13). The only nonzero component of the surface current density corresponds to the current along the azimuthal direction and it is connected to the charge density by the standard relation. We have explicitly shown that for the total surface charge one has the relation (14). Note that, for large values of the harmonic n , the part in the field induced by the cylinder is approximated by the field of an effective point charge (10) located on the cylinder surface. In the limit $r_e \rightarrow r_c$, the field of the charge is compensated by its image and the fields in the region $r > r_e$ vanish.

For a charge rotating around a metallic cylinder, the angular density of the radiation intensity on a given harmonic is given by the expression (16). For the radius of the rotation orbit close to the cylinder surface, the radiation intensity vanishes as $(r_e/r_c - 1)^2$. For small angles θ , one has the relation (20) and the radiation intensity behaves as $\sin^{2(n-1)} \theta$. In the problem with the conducting cylinder, the radiation intensity vanishes at zero angle for all harmonics including $n = 1$. For large harmonics of the radiation, under the condition $\beta \sin \theta < 1$, the effects in the radiation intensity induced by the

cylinder, compared with the standard synchrotron radiation, are suppressed by an additional factor (29). For relativistic particles and for radiation angles close to the rotation plane the contribution of the cylinder to the total radiation intensity can be essential for wavelengths much smaller than the distance from the cylinder.

In section 3, we have studied the radiation for a charge rotating around a metallic diffraction grating on a cylindrical surface. The effect of the grating on the radiation intensity is approximated by the surface currents induced on the strips by the field of the rotating charge. The electric and magnetic fields are presented in the decomposed form (47) where the second term is the contribution induced by the grating. For the latter one has the Fourier expansion (43) with the Fourier components (44) and (46). Compared with the case of the solid cylinder, the Fourier expansion in the geometry of a grating contains an additional summation over m . This corresponds to the periodic structure along the azimuthal direction. At large distances from the grating, the spectral-angular density of the radiation intensity is given by the formula (52) with the functions $R_{n,m}^{(\alpha)}$ defined in accordance with (53). The second term in the right-hand side of (53) determines the contribution of the Smith-Purcell radiation. In two limiting cases $a \rightarrow 0$ and $b \rightarrow 0$, the expression (52) coincides with the exact results for the radiation in a homogeneous medium and for the radiation from a charge rotating around a solid cylinder. Unlike to these limiting cases, the radiation intensity for the geometry of diffraction grating on the harmonics $n > 1$ does not vanish for small angles θ . The corresponding leading term is given by (55).

For a charge rotating around a diffraction grating, the behavior of the radiation intensity on large harmonics n can be essentially different from that for a charge rotating in the vacuum or around a solid cylinder. For a given radiation direction θ , under the conditions $\beta \sin \theta < 1$ and $n \gg 1/\eta_1(\beta \sin \theta)$, the part in the radiation intensity corresponding to the pure synchrotron radiation is exponentially suppressed and, for the impact parameter obeying the condition (56), the total intensity is dominated by the Smith-Purcell part. These features are illustrated in figures 5-7 where the dependence of the angular density of the number of the radiated quanta is depicted as a function of θ for various values of the parameters in the problem. With decreasing energy, the relative contribution of the synchrotron radiation decreases and the Smith-Purcell part is dominant. In particular, the numerical analysis shows that, for given characteristics of the charge, by the choice of the parameters of the diffraction grating, one can have highly directional radiation on a given harmonic directed near the normal to the plane of the charge rotation. For large values of the radiation harmonic and of the number of periods in the diffraction grating, the main contribution to the radiation intensity comes from the term in the summation over m with the lowest value for $|n + mN + \alpha|$ and the locations of the angular peaks in the radiation intensity are not sensitive to the values of the ratio b/a . In addition, for the angles θ not too close to the rotation plane and for high-energy particles, the heights and the locations of the angular peaks are not sensitive to the value of the charge energy.

References

- [1] A.A. Sokolov and I.M. Ternov, *Radiation from Relativistic Electrons* (ATP, New York, 1986).
- [2] *Synchrotron Radiation Theory and Its Development*, edited by V.A. Bordovitsyn (World Scientific, Singapore, 1999).
- [3] A. Hofmann, *The Physics of Synchrotron Radiation* (Cambridge University Press, Cambridge, 2004).
- [4] G.N. Afanasiev, *Vavilov-Cherenkov and Synchrotron Radiation* (Kluwer Academic Publishers, Dordrecht, 2004).

- [5] Ph. Willmott, *An Introduction to Synchrotron Radiation: Techniques and Applications* (John Wiley & Sons, United Kingdom, 2011).
- [6] V.N. Tsytovich, *Westnik MGU* **11**, 27 (1951).
- [7] K. Kitao, *Progr. Theor. Phys.* **23**, 759 (1960).
- [8] T. Erber, D. White, and H.G. Latal, *Acta Phys. Austriaca* **45**, 29 (1976); J. Schwinger, W.-Y. Tsai, and T. Erber, *Ann. Phys.* **96**, 303 (1976); T. Erber, D. White, W.-Y. Tsai, and H.G. Latal, *Ann. Phys.* **102**, 405 (1976); T.M. Rynne, G.B. Baumgartner, and T. Erber, *J. Appl. Phys.* **49**, 2233 (1978); K.T. Bonin, K.T. McDonald, D.P. Russell, and J.B. Flanz, *Phys. Rev. Lett.* **57**, 2264 (1986).
- [9] A.S. Kotanjyan, H.F. Khachatryan, A.V. Petrosyan, A.A. Saharian, *Sov. J. Contemp. Phys.* **35**, 1 (2000); A.S. Kotanjyan and A.A. Saharian, *J. Contemp. Phys.* **37**, 135 (2002); A.S. Kotanjyan and A.A. Saharian, *Mod. Phys. Lett. A* **17**, 1323 (2002); A.A. Saharian and A.S. Kotanjyan, *J. Contemp. Phys.* **38**, 288 (2003); A.A. Saharian and A.S. Kotanjyan, *Nucl. Instrum. Methods Phys. Res., Sect. B* **226**, 351 (2004).
- [10] A.A. Saharian and A.S. Kotanjyan, *J. Phys. A: Math. Gen.* **38**, 4275 (2005); A.A. Saharian, A.S. Kotanjyan., and M.L. Grigoryan, *J. Phys. A* **40**, 1405 (2007); A.A. Saharian and A.S. Kotanjyan, *J. Phys. A* **42**, 135402 (2009); A.S. Kotanjyan and A.A. Saharian, *Int. J. Mod. Phys. B* **26**, 1250033 (2012); A.S. Kotanjyan and A.A. Saharian, *Nucl. Instrum. Methods Phys. Res., Sect. B* **309**, 177 (2013); A.S. Kotanjyan and A.A. Saharian, *J. Phys.: Conf. Ser.* **517**, 012025 (2014).
- [11] V.P. Shestopalov, *The Smith-Purcell Effect* (Nova Science Publishers, New York, 1998).
- [12] A.P. Potylitsyn, M.I. Ryazanov, M.N. Strikhanov, and A.A. Tishchenko, *Diffraction Radiation from Relativistic Particles* (Springer, Berlin, 2011).
- [13] A.R. Mkrtchyan, L.Sh. Grigorian, A.A. Saharian, and A.N. Didenko, *Zhurnal Tekh. Fiz.* **61**, 21 (1991); A.R. Mkrtchyan, L.Sh. Grigorian, A.A. Saharian, and A.N. Didenko, *Acustica* **75**, 184 (1991); A.A. Saharian, A.R. Mkrtchyan, L.A. Gevorgian, L.Sh. Grigoryan, and B.V. Khachatryan, *Nucl. Instrum. Methods Phys. Res., Sect. B* **173**, 211 (2001); A.R. Mkrtchyan, L.Sh. Grigoryan, and A.A. Saharian, *J. Phys.: Conf. Ser.* **517**, 012021 (2014).
- [14] A.R. Mkrtchyan, A.P. Potylitsyn, V.R. Kocharyan, and A.A. Saharian, *Phys. Rev. E* **93**, 022117 (2016).
- [15] H.P. Bluem, R.H. Jackson, Jr., J.D. Jarvis, A.M.M. Todd, J. Gardelle, P. Modin, and J.T. Donohue, *IEEE Trans. Plasma Sci.* **43**, 3176 (2015).
- [16] A.S. Kotanjyan and A.A. Saharian, *Sov. J. Contemp. Phys.* **36**, 310 (2001); A.S. Kotanjyan and A.A. Saharian, *J. Phys. A: Math. Theor.* **40**, 10641 (2007).
- [17] M. Abramowitz and I.A. Stegun, *Handbook of Mathematical Functions* (Dover, New York, 1972).
- [18] D.V. Karlovets and A.P. Potylitsyn, *Phys. Rev. ST Accel. Beams* **9**, 080701 (2006).
- [19] J. Walsh, K. Woods, and S. Yeager, *Nucl. Instrum. Methods Phys. Res., Sect. A* **341**, 277 (1994).
- [20] J.H. Brownell, J. Walsh, and G. Doucas, *Phys. Rev. E* **57**, 1075 (1998).
- [21] D.V. Karlovets and A.P. Potylitsyn, *Phys. Lett. A* **373**, 1988 (2009); D.V. Karlovets and A.P. Potylitsyn, arXiv:0908.2336; D.V. Karlovets, *JETP* **113**, 27 (2011).